Chapter 3

Laser-induced fluorescence in low-pressure flames

In this chapter the theoretical and experimental aspects of laser-induced fluorescence in low-pressure flames are discussed.

3.1 Introduction

In this thesis, spectroscopic techniques are used for measuring temperature and species involved in the mechanism of NO formation. Laser-induced fluorescence (LIF) is one of the most widely used laser spectroscopic techniques for measuring minor species concentrations and flame temperatures in low-pressure combustion processes. We will use it to measure the concentrations of OH, CH and NO, and flame temperature. The method is based on measuring the spontaneously emitted light from a molecule after its excitation to an excited state by absorption of laser radiation. Usually, LIF is performed in the visible and ultraviolet spectral regions.

One of the reasons for the success of LIF is its ability to detect flame species at ppm and even sub-ppm levels, the concentration range of flame species such as OH, CH and NO. Another important advantage is that LIF offers potentially high spatial resolution, which allows obtaining reliable data in regions of steep gradients, giving more detailed information on flame structure. In addition, LIF detection offers high selectivity, low background signal and a simple experimental implementation in comparison with other laser spectroscopic techniques, such as CARS [1-3]. In addition to these advantages, and particularly over traditional probe methods, is that LIF is in principle non-invasive. However, the interpretation of the LIF signal for measurement of temperature and species concentration is often difficult and requires detailed knowledge of collisional processes. This often necessitates an additional calibration method for species concentration measurements.

This chapter begins with a discussion on general theoretical aspects of linear LIF for determination of temperature and OH, CH and NO concentrations in low-pressure flames, followed by an overview of the optical scheme used during the measurements. Finally, the LIF measurements in the "reference" flame [4,5], used to quantify the measurements in the flames studied in this thesis, are described.

3.2 General theory of linear LIF

The important processes involved in LIF are illustrated in Figure 3.1, where a molecule in a single rovibrational level is excited from a lower electronic state to an upper electronic state by laser radiation. Here it is assumed that prior to laser irradiation the population in the excited state is negligibly small. Note that the laser-coupled states are indicated with *u* and *d* for upper and lower rovibrational state, respectively. The excited molecule may undergo spontaneous emission (A_u), which competes with stimulated emission (b_{ud}) and quenching (Q_u, see discussion below). However, other processes that can occur from the excited state are photoionization (W_{ion}) or predissociation (P_k).

Collisions with other molecules distribute the population of the laser-coupled upper rovibrational level, N_u, over other rotational levels in the same electronic-vibrational state (rotational relaxation *R*, see Figure 3.1). Since in the majority of applications transitions are chosen between the lowest vibrational states are used in LIF excitation, so-called (0,0) transitions, in our analyses we neglect collisional transitions to other vibrational levels of the same electronic state (vibrational relaxation). As a consequence of rotational relaxation, fluorescence observed by the detection system may not be emitted from the laser-coupled upper rotational level alone, but also from other rotational levels in the excited state. The temporal fluorescence signal, *I* [photons/sec], collected by the detection system can be expressed as:

$$I = \frac{\Omega}{4\pi} V \sum_i \left[N_i' \sum_j A_{ij} \right], \qquad (3.1)$$

where $\frac{\Omega}{4\pi}$ is the solid angle detected, N_i' is population of rotational level *i* in the upper electronic state, and A_{ij} is the spontaneous emission rate from i^{th} rotational level in upper electronic state to j^{th} rotational level in lower electronic state; the probed volume in the flame $V = l \times S$ [cm^3] is expressed through the laser beam cross-section S and the path length l from which fluorescence is observed by the collecting optics. Since the spontaneous emission rate is a weak function of the rotational level and rotational relaxation primarily occurs to levels close to the initially pumped level [6,7], it can be assumed that:

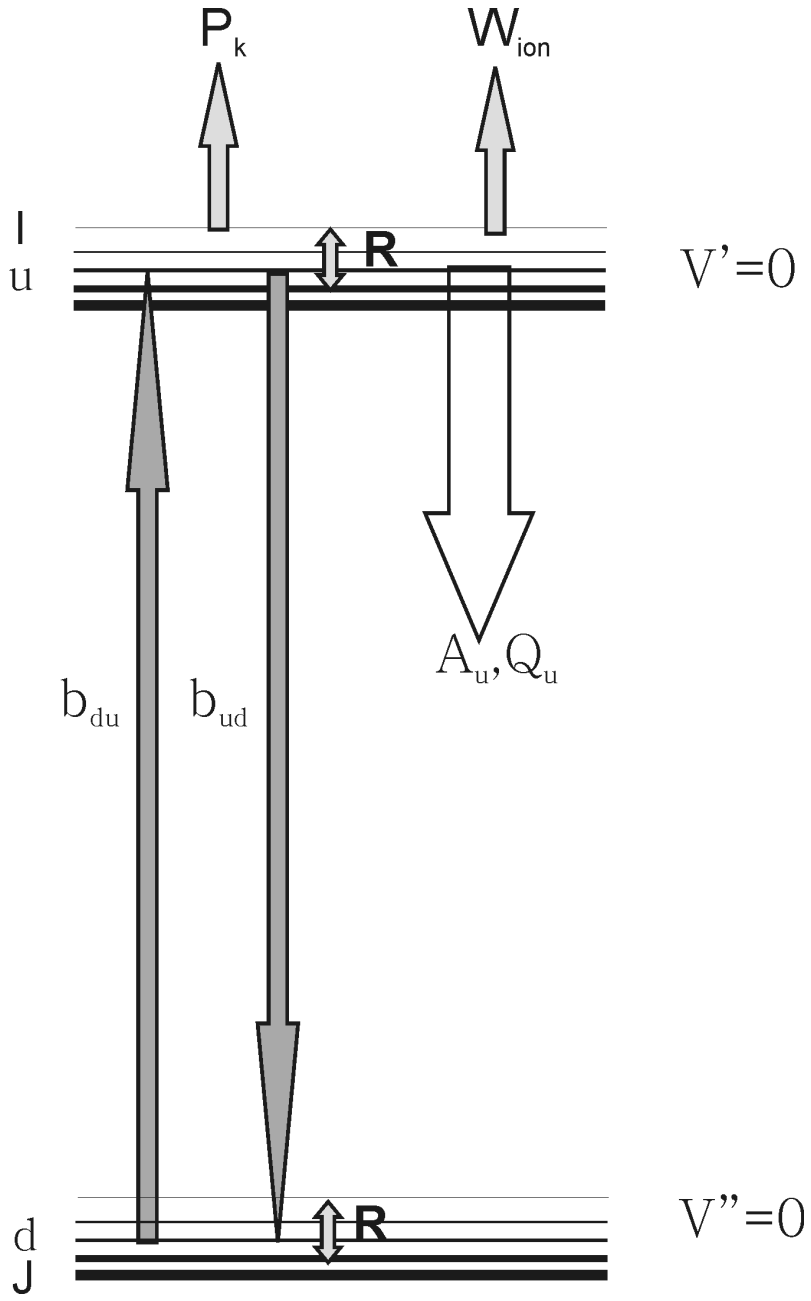

Figure 3. 1 Excitation scheme used for LIF modeling. The laser radiation excites a molecule in a single rotational level d in the v"=0 ground state to rotational level u in the v'=0 excited state. Other rotation levels are indicated with J, the quantum number describing the rotational structure. After excitation, the upper rotation level may undergo rotation relaxation (*R*), vibrational relaxation (*V*), quenching (Q_u), spontaneous emission (A_u), stimulated emission (b_{ud}), photoionisation (W_{ion}) or predissociation from level k (P_k).

$$\sum_j A_{ij} \approx \sum_j A_{uj} = A_u \tag{3.2}$$

Using equations (3.1) and (3.2), the following expression for the temporal fluorescence signal can be found:

$$I(t) = \frac{\Omega}{4\pi} V \cdot N_A'(t) A_u , \tag{3.3}$$

where $N_A' = \sum_j N_j'$ is the total population in the upper excited state. As can be seen from equation (3.3), if all transitions from the excited electronic state are detected, the signal is not affected by rotational relaxation. This is often referred to as broadband detection and is used for the experiments described in this thesis.

To retrieve information on local flame temperature and species concentrations from equation (3.3), it is necessary to describe the dynamics of the excitation process by solving the following system of equations (see also Figure 3.1 [8]):

$$\frac{dN_k'}{dt} = \sum_j N_j'' b_{jk} + \sum_{i \neq k} N_i' R_{ik}' - N_k' \left[\sum_{i \neq k} \left(b_{ki} + R_{ki}' \right) + Q_u + A_u + P_k + W_{ion} \right], \tag{3.4}$$

$$\frac{dN_m''}{dt} = -N_m'' \sum_j b_{mj} + \sum_{j \neq m} R_{jm}'' N_j'' - N_m'' \sum_{j \neq m} R_{mj}'' + N_j'' Q_d , \tag{3.5}$$

where subscript *k (=i or u)* and *m(=j or d)* denote rotational levels in the upper and lower electronic state, respectively, N_k' is population of k^{th} rotational level of the upper electronic state, N_m'' is population of m^{th} rotational level of lower electronic state, b_{ji} and b_{ij} are the rates of absorption and stimulated emission, respectively,

$$b_{ij} = b_{ji} = 0 \text{ for } i \neq u,d \text{ and } j \neq u,d ,$$

$R_{ik}^{'}$ is the rate of collisional transfer between the ith and kth rotational levels of the upper electronic state, P_k is rotational level dependent predissociation rate, W_{ion} is the photoionisation rate and Q_u is the total quenching rate for level u:

$$\sum_j Q_{ij} \approx \sum_j Q_{uj} = Q_u \ .$$

The rates b_{du} and b_{ud} are related to the Einstein coefficients for absorption and spontaneous emission (B_{ij} [cm^{2}J^{-1}s^{-1}]), respectively, through [2]:

$$b_{ij} = \frac{B_{ij} I_L(t) \cdot \Gamma(v)}{c}, \qquad (3.6)$$

where $I_L(t)$ is the laser irradiance [Wcm^{-2}], c is the speed of light [cm.s^{-1}] and $\Gamma(v)$ [cm] is the convolution integral that describes the overlap between the absorption $g_A(\nu\text{-}\nu_{ji})$ and laser line $g_L(\nu\text{-}\nu_L)$ profiles (see below),

$$\Gamma(v) = \int_{-\infty}^{+\infty} g_A(v - v_{ji}) \cdot g_L(v - v_L) dv \ , \qquad (3.7)$$

where v_0 is the frequency of the line center of molecular transition [cm^{-1}] and v_L is the laser line center [cm^{-1}]. The absorption line profile for transition between j^{th} and i^{th} level [cm] depends on pressure, temperature and composition [2,8]. $\Gamma(v)$ is a complicated function and is usually determined experimentally (see below).

To simplify the further analysis, we neglect P_i and W_{ion}. This assumption is valid for moderate laser intensities and excitation laser frequencies below the dissociation limit. The expression for the time dependence of the total population $N_A^{'}$ is acquired by summation of equation (3.4) over all rotational levels of the upper electronic state:

$$\frac{dN_A^{'}}{dt} = N_d^{"} b_{du} - N_u^{'} b_{ud} - N_A^{'}(t)(A_u + Q_u). \qquad (3.8)$$

In this work we consider the case of low laser intensities for which we can neglect the terms $N_u^{'} b_{ud}$ and $N_d^{''} b_{du}$ in equation (3.5). In this approximation, the distribution in the ground electronic state is Boltzmann. Then, equation (3.8) can be rewritten as

$$\frac{dN_A^{'}}{dt} = f_d N_{tot} b_{du} - N_A^{'}(t)(A_u + Q_u), \tag{3.9}$$

where f_d is the Boltzmann fraction of rotational level d and N_{tot} is the total population in the system $\left(= N_d^{''} + N_A^{'}\right)$.

The values of A_u, b_{du} and b_{ud} in equation (3.9) can be found through tabulated Einstein coefficients [9] and Q_u can be either calculated for known composition using published cross-sections [10] or determined directly from experiments, as will be discussed below.

Integrating equation (3.9) over time, the following expression can be found:

$$0 = f_d N_{tot} \int_0^\infty b_{du} dt - (A_u + Q_u) \int_0^\infty N_A(t) dt\,. \tag{3.10}$$

An expression for the time-integrated LIF signal, I_v [photons] can be found by using equations (3.3) and (3.10):

$$I_v = \int I(t) dt = l \frac{\Omega}{4\pi} \phi_u \frac{B_{du}}{c} f_d(T) \frac{X_i P}{kT} E_L \cdot \Gamma(v), \tag{3.11}$$

where $\phi_u = A_u / (A_u + Q_u)$ is the fluorescence quantum yield and $E_L = S \int I_L(t) dt$ is the laser energy and S laser beam cross section. As can be seen from equation (3.11), the time-integrated LIF signal is linearly proportional to the laser energy, hence the name "linear LIF".

Integrating equation (3.11) over frequencies, the fluorescence signal F [Photons] can be written as:

$$F = l \frac{\Omega}{4\pi} \phi_u \frac{B_{du}}{c} f_d(T) \frac{X_i P}{kT} E_L, \tag{3.12}$$

An advantage of using the integrated area under a peak is that information on the convolution integral $(\Gamma(v))$ is not needed.

3.2.1 LIF excitation spectra for OH, CH and NO

To identify species, scanning of the excitation wavelength in particular spectral region is performed. Figure 3.2 shows examples of theoretically generated excitation scans for OH, CH and NO molecules. Clearly, the spectra shown in Figure 3.2 are distinct for each molecule and spectral line assignments can be done.

The spectral features selected for determination of OH, CH [5] and NO concentration should be spatially resolved, free from interference from other lines in the spectrum, and their intensity should allow quantitative measurement at low concentrations. Table 3.1 summarizes the transitions excited, identity of electronic-vibrational bands and wavelengths used for determination of the OH, CH and NO concentration:

Species	Transition	Band	λ, nm
OH	$R_2(6.5)$	$A^2\Sigma^+$-$X^2\Pi$ (0,0)	306.9
CH	$P_{1e}(8.5)$	$A^2\Delta$-$X^2\Sigma$ (0,0)	435.4
NO	$Q_1(16.5)$	$A^2\Sigma$-$X^2\Pi$ (0,0)	225.95

Table 3. 1 Excitation scheme for detecting OH, CH and NO. The rotational transitions are also indicated by arrows in Figure 3.2.

As mentioned above, the value of F in equation (3.12) is determined using the area under a peak. Other parameters are known (*c, k* and *P*) or can be found in spectroscopic tables (A_u and B_{du}) and the laser energy is measured. However, the temperature, quenching rate and geometric factor $l\frac{\Omega}{4\pi}$ are unknown and depend on the experimental conditions used.

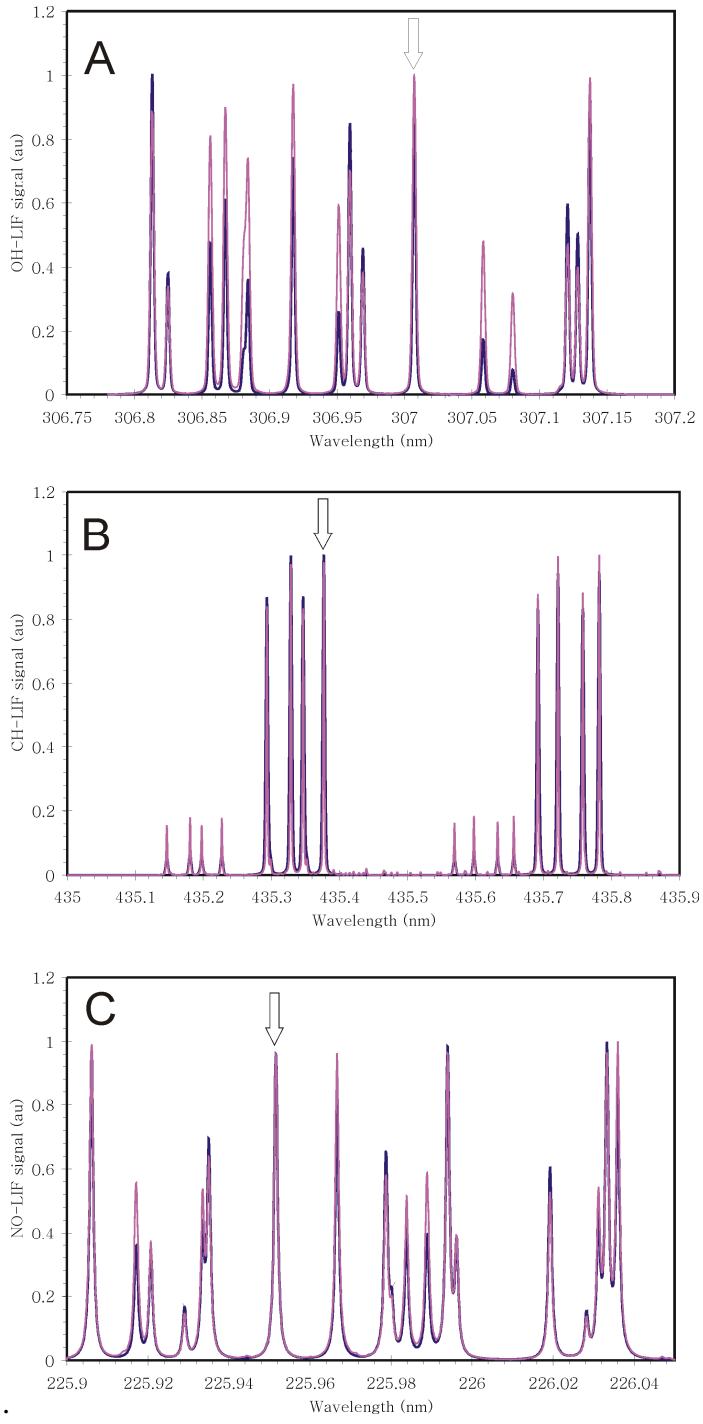

Figure 3. 2 Theoretical OH-LIF (A), CH-LIF (B) and NO-LIF (C) spectra for *T* = 1500 (blue line) and 2500 K (red line). The above spectra are calculated using LIFBASE program [9]. The arrows indicate the transitions used in this study.

3.2.2 Concentration determination in a flame

The absolute concentration of species *i* from the LIF signal (*F*) can be determined by calibration. The calibration methods applied for the experiments described in this work is the use of a reference flame [4,5]: a flame with known concentration of species *i* and corresponding temperature. In this case the LIF signal from the target flame is compared to the LIF signal from the reference flame, using in both cases the same rotational transition and detection scheme:

$$X_i = X_{i,cal} \cdot \left(\frac{F}{F_{cal}} \right) \cdot \left(\frac{E_L}{E_L^{cal}} \right) \cdot \left(\frac{\phi_{u,cal} \cdot P_{cal}}{\phi_u \cdot P} \right) \cdot \left(\frac{f_d(T_{cal}) \cdot T}{f_d(T) \cdot T_{cal}} \right), \qquad (3.13)$$

where the subscript cal denotes calibration. The geometrical factor is cancelled out and only temperature, pressure, quenching, laser power and fluorescence intensities have to be determined for acquiring absolute concentrations. Of course, to apply this calibration method, the concentrations of the species of interest in the reference flame have to be determined first.

One of the methods for determination of the concentration in the reference flame is direct absorption [11,12]. This spectroscopic technique is most widely used to calibrate the LIF signal. Basically, direct absorption is based on the first step in LIF. An atom or molecule is excited by absorption of laser radiation, and the attenuation in the laser beam caused by the absorption as the beam passes through the flame is measured. If the spectroscopic constants of the absorbing species are known, the concentration of the absorbing species can be determined directly. This calibration method for LIF has been used successfully in our laboratory for determination of OH in atmospheric pressure CH_4/Air flames [11]. However, since the attenuation of the laser beam due to absorption is cumulative through the absorbing medium, direct absorption measurements require information on spatial distribution of the measured species. At low pressure, particularly the presence of absorbing species in the circulating gases between the flame and the walls of the combustion chamber render this method difficult to use [13]. As such, we have chosen not to used it in the present study.

Another way of determining the absolute concentration in the reference flame is by seeding the cold-gas mixture with known quantities of species.

When the cold-gas mixture is seeded with NO, it is assumed that the seeded NO is conserved in the flame front [14]. This method is used for the measurement of NO concentration in our low-pressure reference flame following the description by Berg et al. [4], as will also be discussed below. The advantage of this method is that the spatial distribution of NO in flame is not needed, since only LIF is used as measurement technique.

Unfortunately, the methods described above cannot be used for determination of absolute CH concentrations in the reference flame, since it is present at concentrations too low for direct absorption [15], and, as very reactive molecule, CH cannot be added to the unburned fuel/oxidizer mixture. Luque et al. [15] proposed a method of calibration using Rayleigh scattering, which will be discussed in § 3.4.4

3.2.3 LIF thermometry

The temperature is one of the key parameters in combustion science, since flame chemistry is strongly temperature dependent. In addition, the local temperature is needed for quantifying the species data obtained by LIF and for analysis of the results.

The influence of the temperature on the excitation spectra OH, CH and NO is illustrated in Figure 3.2, where spectra are calculated for two different temperatures: T= 1500 and 2500 K. Since the spectra shown in Figure 3.2 are sensitive to changes in temperature, it should be possible to retrieve a temperature from the measured excitation spectrum.

The temperature can be determined using the relation between the Boltzmann fraction of a rotational level J in a single vibrational state f_J and the temperature:

$$f_J = \frac{(2J+1)}{Q_{rot}(T)} \exp\left[-\frac{hcE_J}{kT}\right], \qquad (3.14)$$

where Q_{rot} is the rotational partition function and E_J is the rotational energy for level J. Equation (3.12) can be rewritten using the above equation:

$$\ln\left[\frac{F}{(2J+1)\phi_u B_{du}(J)E_L}\right] = -\frac{E_J}{kT} + C\,, \qquad (3.15)$$

where C is a constant. When the left side of equation (3.15) is plotted as function of E_J/k, a straight line is obtained with a slope equal to $-1/T$. An example of this "Boltzmann plot" from data taken in this thesis is shown in Figure 3.3.

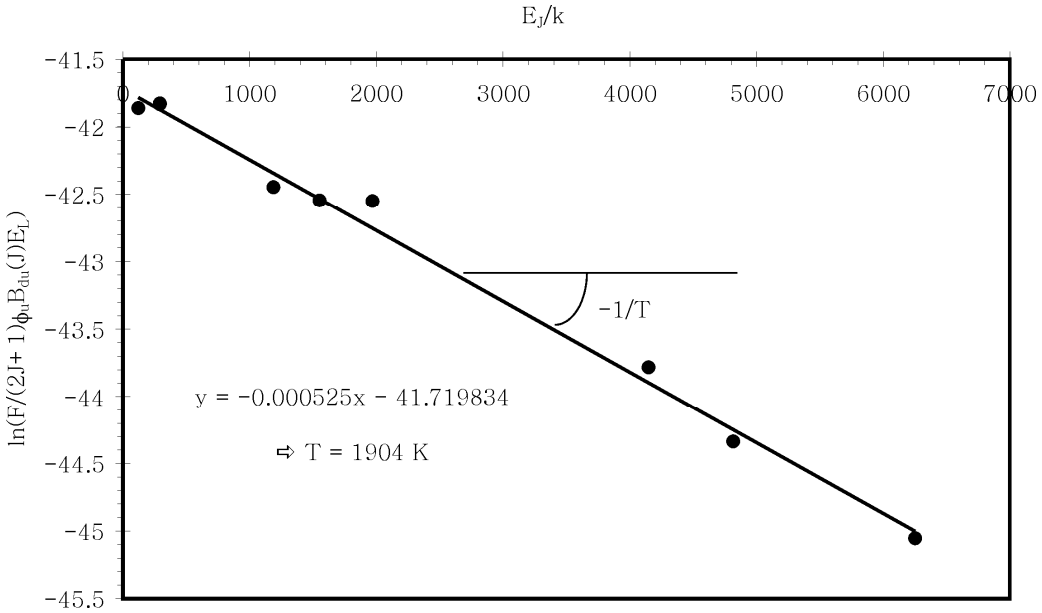

Figure 3. 3 Boltzmann plot for determination of the temperature in a premixed $CH_4/O_2/N_2$ flame (ϕ=1.07. ρv=0.0023 g/cm^{2}s, p=25 Torr, $[O_2]/[O_2]+[N_2]$ =0.30, 1.42 cm above burner surface)

Thus, the temperature in a flame can in principle be determined from the excitation scan of OH [16], CH [17] or NO [18]. However, the CH radical is present at low concentrations and only in the flame front, which makes it impossible to measure temperatures downstream in the flame where NO mole fraction reaches its maximum. Furthermore, temperature measurements using CH are restricted to only hydrocarbon flames. Since the rotational constant for NO is much smaller than for OH (and CH) [9] it is difficult to resolve individual transitions, which is needed for temperature determination. Moreover, when performing LIF measurements on NO, special care must be taken to avoid interference from lines arising from O_2 transitions in the

Schumann-Runge system [19,20]. Finally, the NO-LIF spectra shown in Figure 3.2 appear to be less sensitive to temperature variations in comparison to the OH-LIF spectra.

The best candidate for determining the temperature using LIF is therefore the OH radical. In fact, it is one of the most frequently used species for performing LIF thermometry, especially in low-pressure flames [16]. Besides the large rotational constant, another advantage of the OH radical is its presence at substantial concentrations in nearly all parts of hydrocarbon and hydrogen flames. The rotational transitions in the $A^2\Sigma^+$-$X^2\Pi$ band of OH used in a Boltzmann plot for determination of the temperature are indicated in Figure 3.4 [16]:

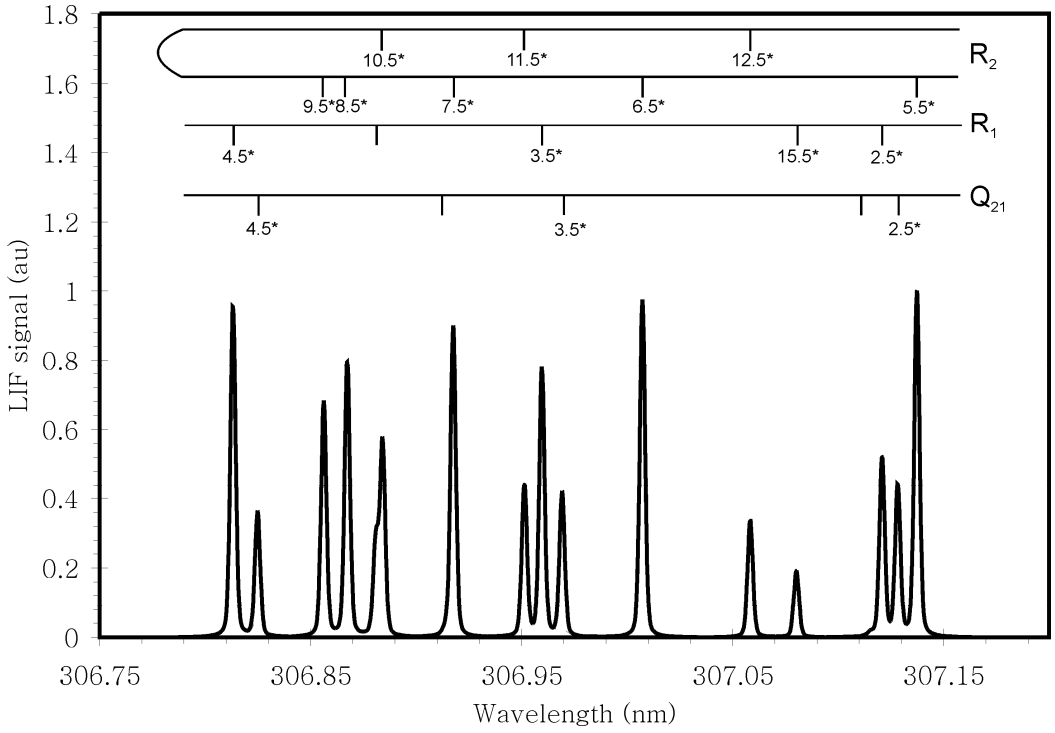

Figure 3. 4 Overview of the rotational transitions in the part of the OH-LIF spectrum used for temperature measurements. The rotational transitions used for constructing a Boltzmann plot are indicated with an asterisk (*).

One of the transitions used for determination of the temperature is also used for OH concentration measurements (see also Table 3.1). Thus, once the quenching rate is known, both temperature and OH concentration can be determined from the same set of data.

3.2.4 Determination of quenching rate (Q_u)

Suppose a molecule or atom is excited using a short laser pulse of duration τ_L and low laser energy. The population of the upper electronic state N_A' then initially builds up in time and reaches some value, $N_A'(\tau_L)$. After laser excitation has ceased, the solution of equation (3.9) becomes

$$N_A'(t) = N_A'(\tau_L)\exp[-(A_u + Q_u)t]. \qquad (3.16)$$

The time dependence of N_A' just described is depicted in Figure 3.5.

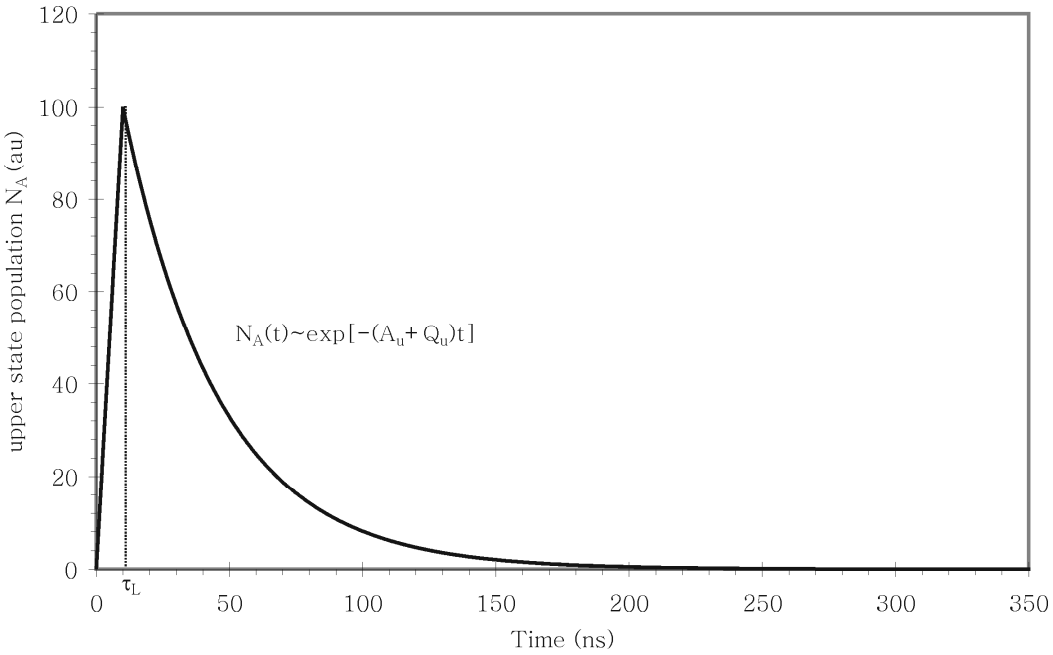

Figure 3. 5 Population v'=0 level population (N_A) during and after excitation by laser radiation. The calculations are performed for OH molecule using a pulse duration τ_L = 10 ns and typical low-pressure combustion values: A_u=0.0028 ns^{-1} and Q_u = 0.025 ns^{-1}.

Fitting the fluorescence decay using equation (3.16) will yield A_u+Q_u and after subtraction of the tabulated spontaneous emission rates [9], the quenching rate is determined. Thus, if the laser pulse duration is short compared to the value of $1/(A_u+Q_u)$, it is possible to measure the quenching rate directly.

3.3 Experimental setup

Figure 3.6 shows a schematic overview of the LIF setup. First, the laser systems used for generating ultraviolet radiation will be discussed and then the detection system.

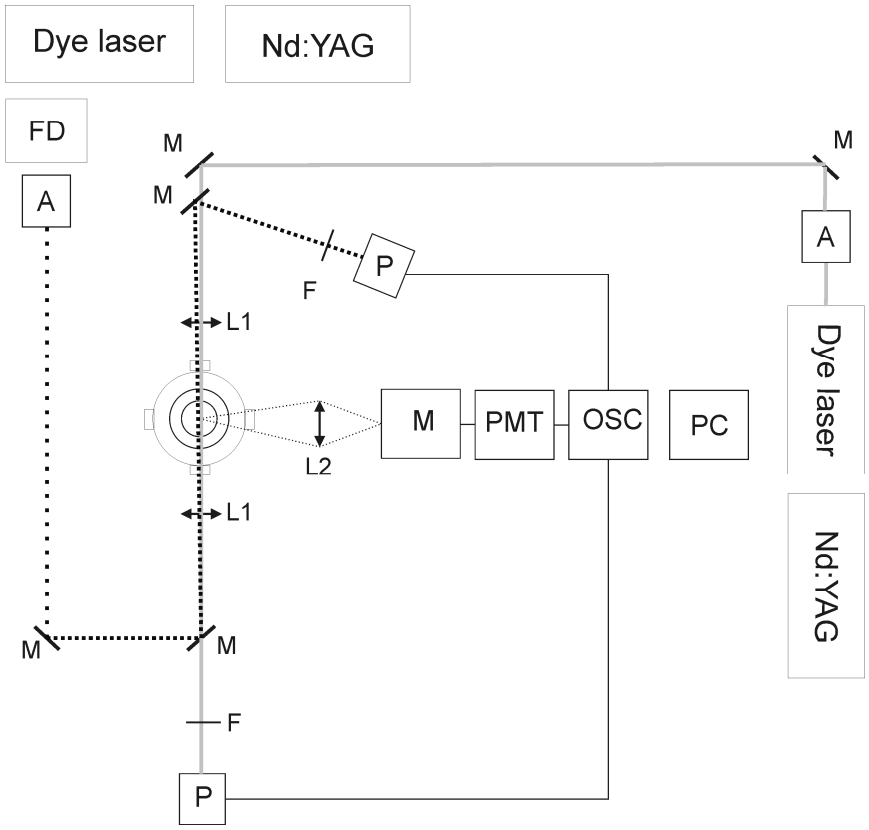

Figure 3. 6 Optical scheme for performing LIF experiments. Code: A. attenuator; F. filter; FD, frequency doubling; L1, L2, lenses; M: mirror; PMT, photomultiplier; PC: personal computer. The grey line represents the laser system used for NO- and CH-LIF experiments and the dotted line for OH-LIF experiments.

3.3.1 Laser systems

The LIF measurements are performed using two laser systems: one for OH concentration and temperature measurements and one for CH and NO concentration measurements. In both systems a tunable dye laser (Sirah PrecisionScan) pumped by a Nd:YAG laser (Spectra Physics Quanta Ray Pro

250-10), with pulse duration of 10 ns, is used as a source of ultraviolet radiation.

Table 3.2 summarizes the dye mixtures and the wavelengths used for generating UV radiation for each specific molecule:

Species	Laser Dye	Ultraviolet radiation (nm)
OH	81% Rhodamine 610 19% Rhodamine 640	307 nm (after frequency doubling)
CH	Coumarin 440	435 nm
NO	DCM	226 nm (after mixing with 3rd harmonic of Nd:YAG laser)

Table 3. 2 Overview of the laser dyes and wavelengths used detection of OH, CH and NO.

The beams from the two lasers entered the vacuum chamber from opposite directions, and two quartz lenses (f=850 mm) focus the beam to the same point in the flame. Two Newport UV-enhanced silicon PIN photodiodes are used for monitoring the energies of the two beams before and after the vacuum chamber (see below).

3.3.2 Detection system

Fluorescence from the center of the flame is collected at right angles by a quartz camera lens (Nikkor f/4.5) and focused onto an Acton Research Corporation SpectraPro 2150i spectrometer (f/4, 10 nm/mm). The spectrometer bandpass is set to 30 nm to capture the entire emission band of the OH A-X(0, 0), CH A-X(0, 0) and NO A-X(0, 3) systems [4,5]. The collection is centered at 312 (OH), 431 nm (CH) and 260 nm (NO). The advantage of the detection system used here is that only the center wavelength of the spectrometer needs to be changed when measuring a different molecule. The fluorescence signals are detected by an Electron Tubes 9659QB photomultiplier. The entrance slit of the spectrometer is parallel to the laser beam. The signal is collected over the center 1.5 cm of the flame. Results obtained previously [21] using an identical burner indicated that this limited region of interrogation should be sufficiently flat for the purposes discussed here. Measurements of the profiles of the OH

mole fraction repeated using the center 0.5 cm of the flame showed identical results to those for 1.5 cm resolution. The vertical spatial resolution is estimated to be better than 0.5 mm (the diameter of the beam waist). At every measurement point the transient fluorescence and laser power signals are digitized and averaged over 8 (temperature), 64 (OH and CH) and 256 (NO) pulses by a 500 MHz Hewlett Packard 54615B oscilloscope, and are stored on a personal computer.

When determining the temperature by exciting the (0-0) OH band, it is necessary to take into account the effects of fluorescence trapping and attenuation of the laser beam. In this work, the photodiode is located after vacuum chamber, to compensate the effects of both attenuation and trapping [22]. These two effects influence the temperature determined from the Boltzmann plot, and will be addressed below.

3.4 Reference flame measurements

To test our calibration method, temperature and OH, CH and NO concentration profiles are measured in a p=25 Torr ϕ=1.07 premixed $CH_4/O_2/N_2$ flame (ρv=0.0023 g/cm^{2}s and $[O_2]/[O_2]+[N_2]=0.30$) which was investigated by Berg et al. [4,5]. This flame will be used as a reference flame for performing measurements in other flames. Since many of the results from this flame were also used as benchmarks for optimizing the GRI-Mech mechanism [23], we suggest that reproduction of these measurements allows a more calibrated comparison between measurements and model predictions. In this paragraph the calibration methods and the results of the measurements in the reference flame will be discussed.

3.4.1 Experimental LIF-spectra and linearity check

In Figures 3.7-3.9 the measured OH-, CH- and NO-LIF spectra are compared with calculated spectra. The good correspondence of the measured spectra with calculations indicates that the measured spectra are free from interference from other components in the flame. The spectra also show that the lines used for determination of the OH, CH and NO concentrations are well separated from other lines.

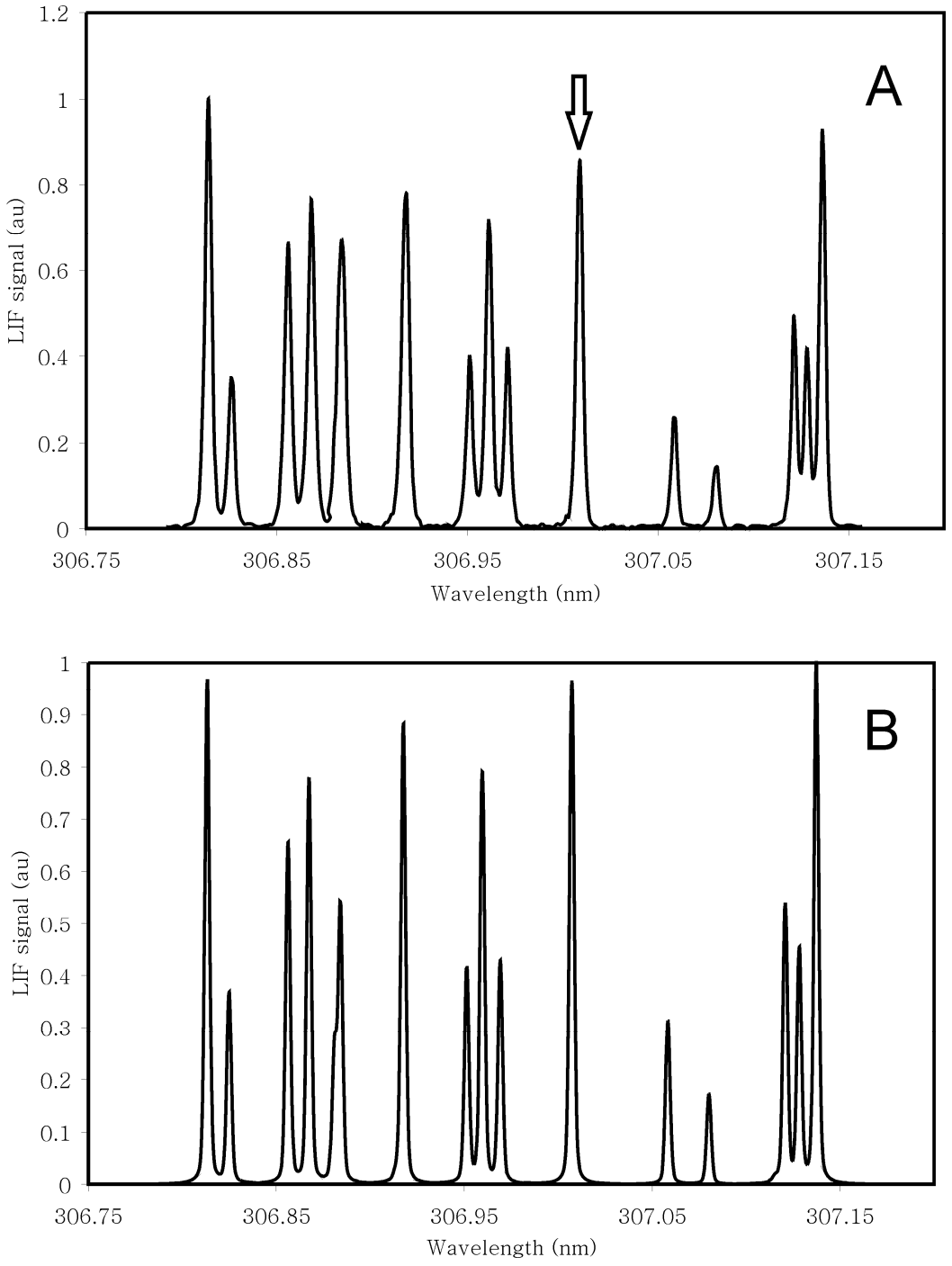

Figure 3. 7 Experimental OH-LIF spectrum (A) for the reference flame at 1.22 cm above the burner surface. The theoretical spectrum (B) is calculated using LIFBASE program [9] for *T*=1920 K. The arrow indicates the $R_2(6.5)$ rotational transition in $A^2\Sigma^+$-$X^2\Pi$ (0,0) band used for measuring OH concentrations (see also Table 3. 2)

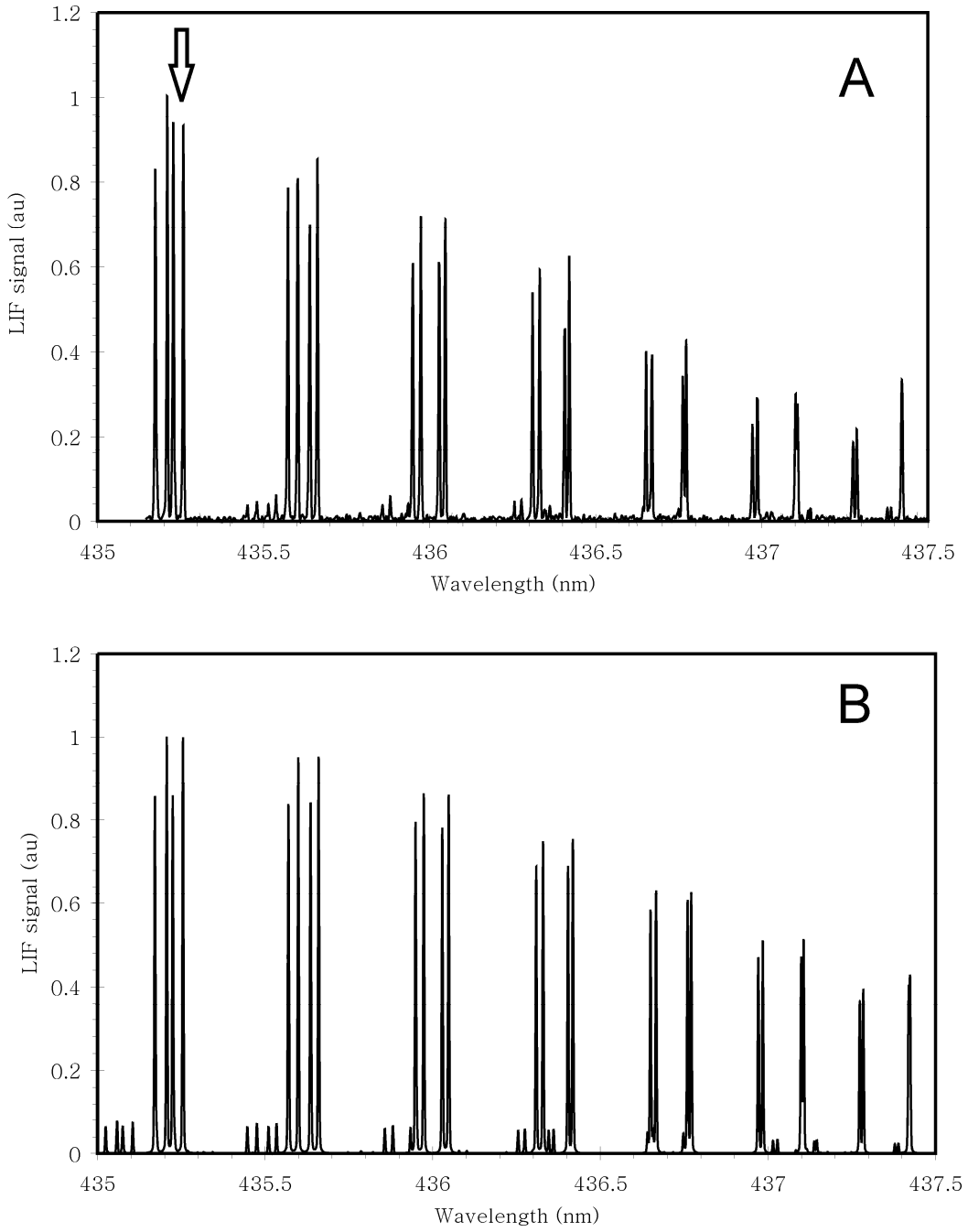

Figure 3.8 Experimental CH-LIF spectrum (A) for a premixed methane-air flame (ϕ=1.13, ρv=0.0018 g/cm^{2}s, p=40 Torr, 1.5 cm above burner surface). The theoretical spectrum (B) is calculated using LIFBASE program [9] for T=1700 K. The arrow indicates the $P_1(8.5)$ rotational transition in $A^2\Delta$-$X^2\Pi$ (0,0) band used for measuring CH concentrations (see also Table 3. 2)

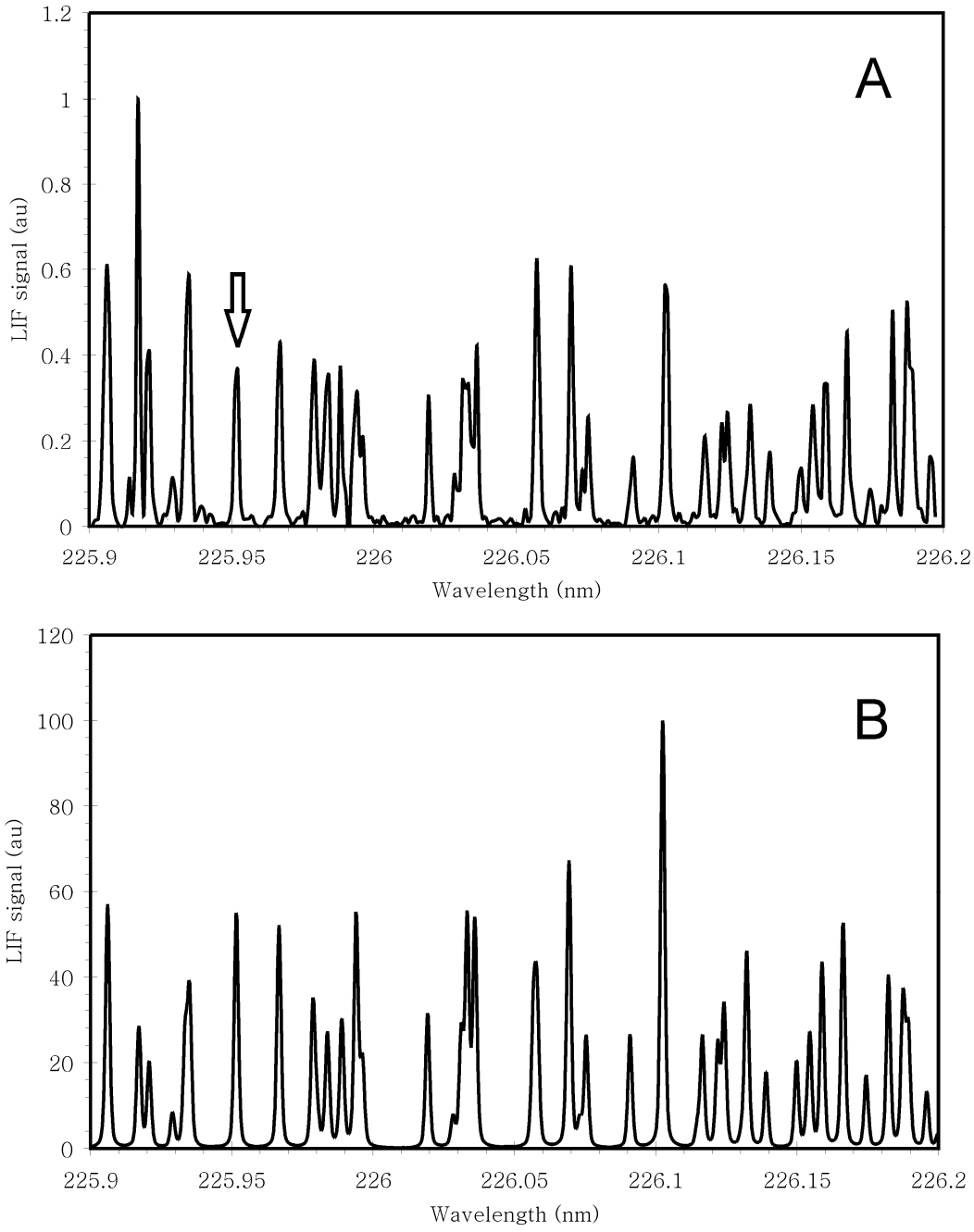

Figure 3.9 Experimental NO-LIF spectrum (A) for a premixed $CH_4/O_2/N_2$ flame (ϕ=1.3, ρv=0.0039 g/cm^{2}s, p=35 Torr,$[O_2]/[O_2]+[N_2]$=0.305, 2 cm above burner surface). The theoretical spectrum (B) is calculated using LIFBASE program [9] for T=1900 K. The arrow indicates the $Q_1(16.5)$ rotational transition in $A^2\Sigma$-$X^2\Pi$ (0,0) band used for measuring NO concentrations (see also Table 3. 2)

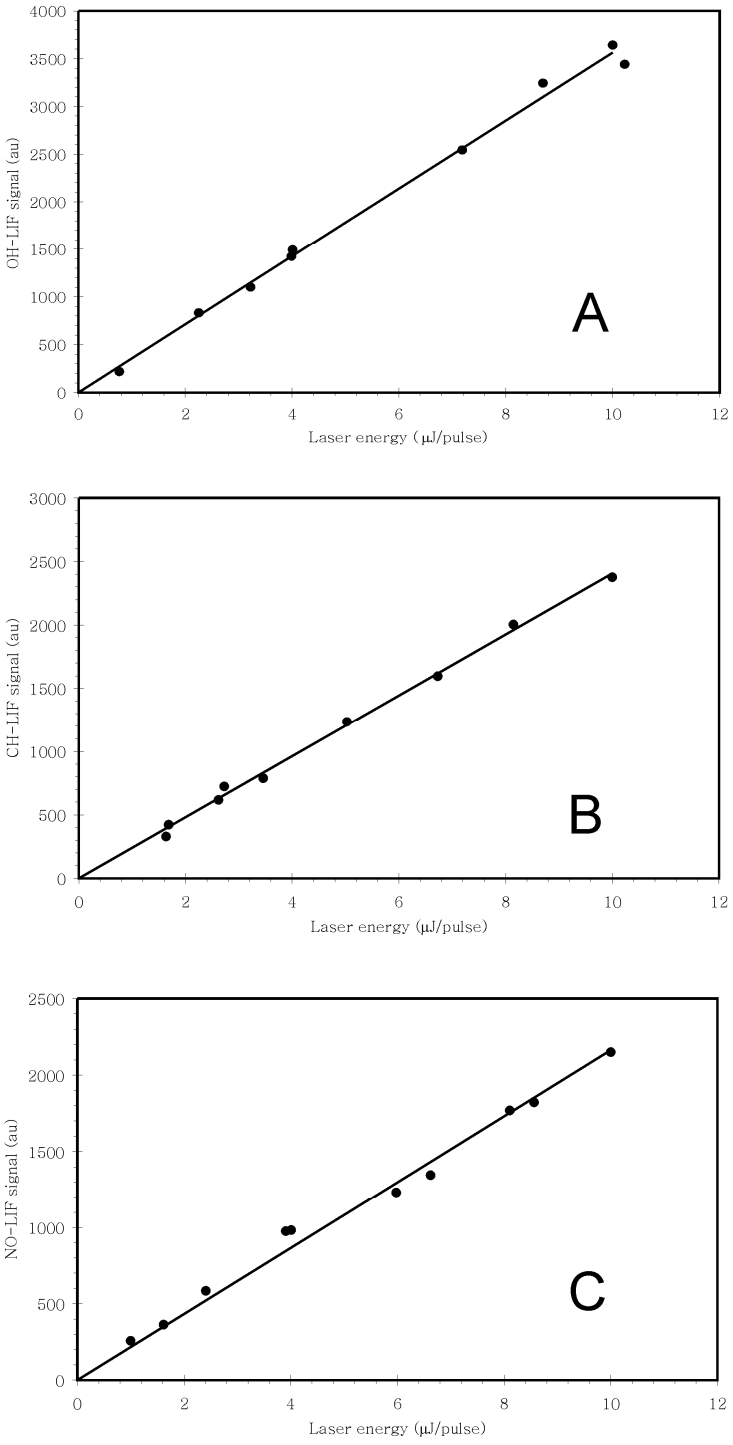

Figure 3. 10 Fluorescence signal for OH(A), CH(B) and NO(C) plotted against the laser energy

Before starting quantitative measurements, it is necessary to verify the linearity of the LIF signal. For this purpose, the fluorescence is measured at different excitation lines listed in Table 3.1, while varying the laser power. The LIF signals for OH, CH and NO plotted as function of the laser energy are shown in Figure 3.10. The results show an excellent linear dependence between the LIF signals and the laser energy.

3.4.2. Quenching rate measurements

The time-dependent signal measured by the detection system $I_M(t)$ is a convolution of the fluorescence intensity $I(t)$ and the instrument function $F(t)$ of the detection system:

$$I_M(t) = \int_{-\infty}^{\infty} I(t-\tau')F(\tau')d\tau', \tag{3.17}$$

If the fluorescence decay time, $\tau_{FL} = 1/(A_u + Q_u)$, is much longer than the characteristic response time of the detection system τ_D, the instrument function can be regarded as a delta function and the measured signal is equal to the fluorescence intensity. The fluorescence decay time for the molecules under investigation, $\tau_{FL} = 1/(A_u + Q_u)$, is approximately 50-70 ns, while the response time of the detection system is of the same order (15 ns [14]). In this case, the fluorescence decay time should be determined by deconvoluting the fluorescence signal from the measured signal. To simplify the deconvolution procedure, the instrument function is approximated as a Gaussian function $\exp\left(-(t-\tau')^2/\tau_D\right)$. After integration the following equation is obtained:

$$I_M(t) = C\exp\left[-\frac{t-t_0}{\tau_{FL}}\right]\cdot erfc\left[-\frac{t-t_0}{\tau_D}-\frac{\tau_D}{2\tau_{FL}}\right], \tag{3.18}$$

where C is a constant and *erfc()* is a complementary error function [24]. Equation (3.18) is fit to the measured temporal fluorescence decay to determine the unknown parameters C, t_0 and τ_{FL} using the subroutine LMDIF from the MINPACK library [25]. An example of such a fit is shown in Figure 3.11.

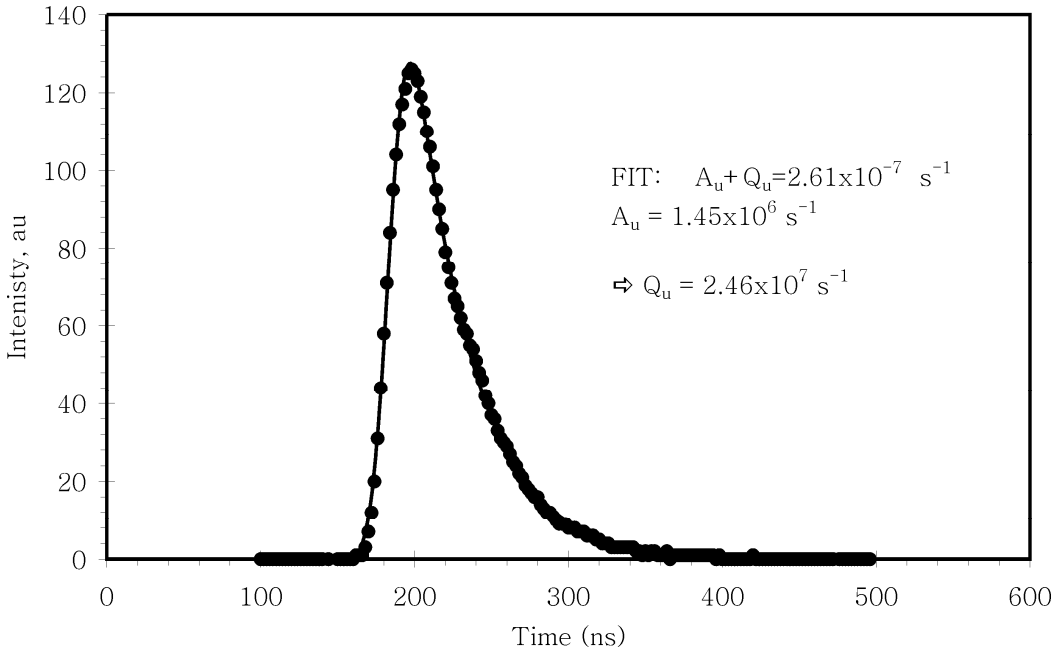

Figure 3. 11 Example of fitting temporal OH-LIF signal for the reference flame at 1.5 cm above the burner surface. The OH-LIF signal is from the $R_2(6.5)$ rotational transition in the $A^2\Sigma^+$-$X^2\Pi$ (0,0) band.

It is possible to calculate the quenching rate by using measured quenching cross sections for the major species and the major species mole fractions obtained from flame calculations. In the study performed by Tamura et al [10], the calculated quenching rates are compared with measurements, and a good agreement is found for OH and NO. However, their calculated CH quenching rates were systematically higher, up to 27 %. The discrepancies in the absolute values of CH quenching rate are probably due to lack of knowledge of high temperature data for N_2 and H_2O colliders [10].

Table 3.3 shows experimentally determined quenching rates for our reference flame and those calculated using the published quenching rates [10] and the temperature profile for the reference flame measured by Berg et al [5]. The quenching rates for OH and NO are taken at 1.5 cm above the burner surface and CH quenching rate at 0.47 cm above the burner surface.

Species	Experimental quenching rate, (10^7 s^{-1})	Calculated quenching rate, (10^7 s^{-1}) [10]
OH	2.45	2.46
CH	1.19	1.06
NO	3.00	2.99

Table 3. 3 Experimental and theoretical quenching rates for OH, CH and NO, where OH and NO quenching rates are taken at 1.5 cm above the burner surface and CH quenching rate at 0.47 cm , which is the location of the CH peak in this flame. The measurements are a result of repeated measurements.

The experimental quenching rates correspond very well with calculated data for OH, CH and NO. Although it is tempting to use the data published by Tamura et al [10] instead of determining the quenching experimentally, the uncertainty in the CH data indicates that experimental determination of local quenching is still needed for accurate concentration determination. Moreover, the data published by Tamura et al [10] do not take into account the dependence of the quenching on rotational level.

Several investigators confirmed this rotational level dependence of quenching, but only a few measurements have been performed in flames [7,26,27]. This dependence is especially important for temperature measurements, where several rotational levels in the excited $A^2\Sigma^+(v'=0)$ level of OH are used (see equation 3.15), in contrast to concentration measurements were only one rotational level is used. The measured dependence of the quenching of OH ($A^2\Sigma^+$,v"=0) upon the rotational quantum number is shown in Figure 3.12. The decrease of the quenching rate with increasing rotational quantum number is consistent with observations for the same electronic-vibrational level of OH by other investigators [7,26].

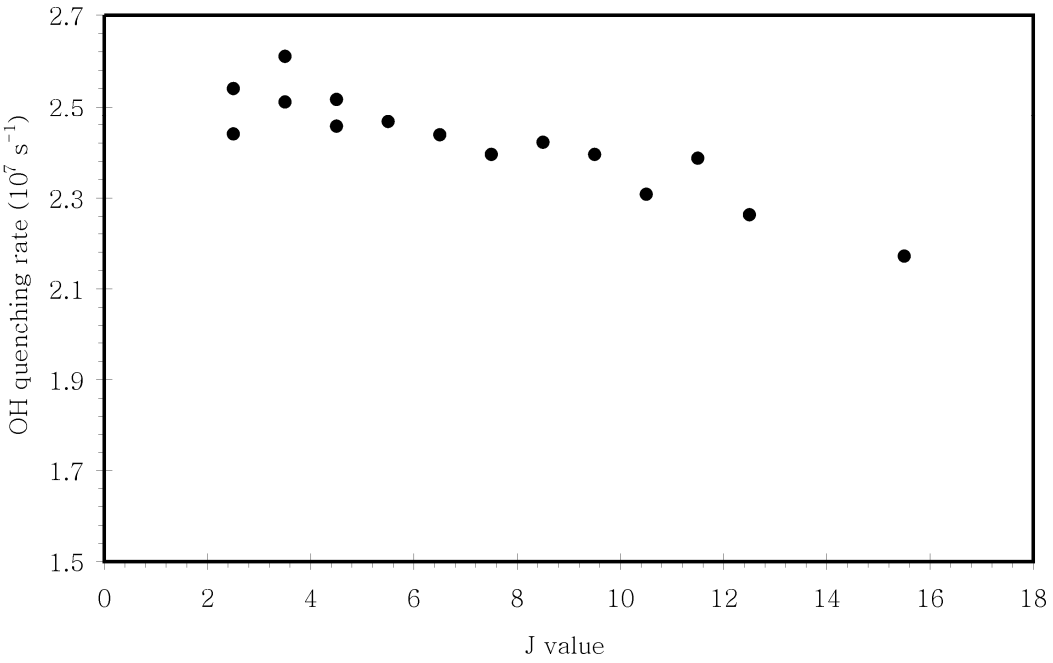

Figure 3. 12 OH quenching rate as function of rotational quantum number The quenching rate is determined at 12 mm above the burner surface in a premixed $CH_4/O_2/N_2$ flame (ϕ=1.07, ρv=0.0023 g/cm^{2}s, p=25 Torr, $[O_2]/[O_2]+[N_2]$=0.30)

3.4.3 Temperature measurements

As mentioned before, a Boltzmann plot is used for determining the flame temperature from rotational excitation scans (see Figure 3.3). Similarly, the temperature is determined for the reference flame at several distances above the burner surface, resulting in a temperature profile as shown in Figure 3.13.

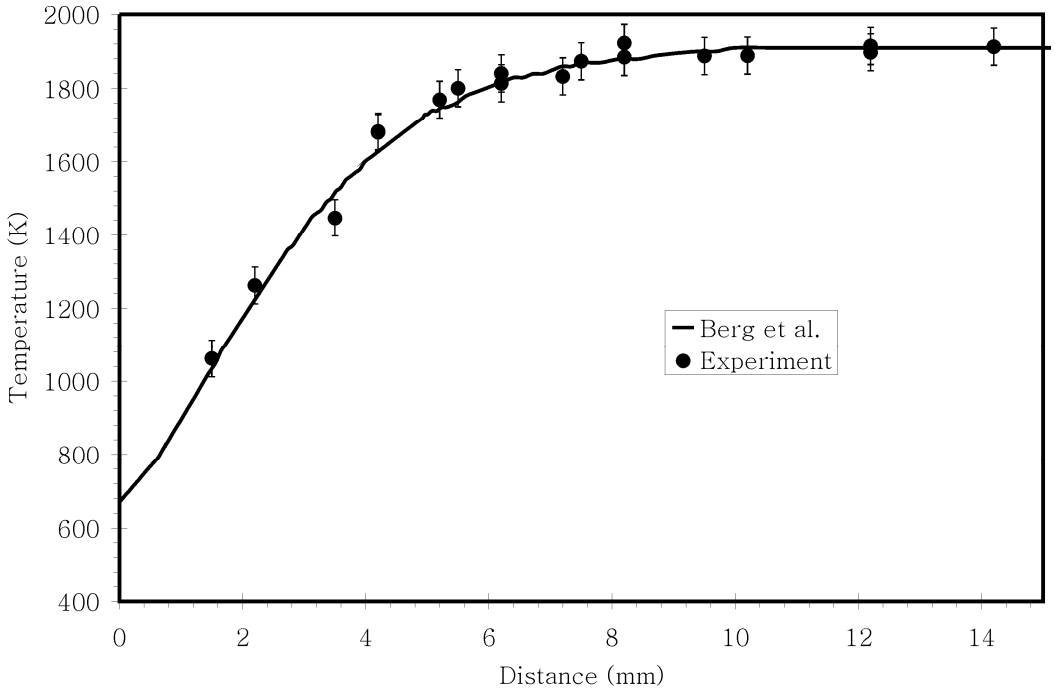

Figure 3. 13 Temperature profile for reference flame. Error bars of 50 K represent an estimation of the maximum error in the temperature measurements. Also the temperature profile measured by Berg et al [5] is shown.

The measured temperature profile agrees within 35 K with the temperature profile measured by Berg et al. [5]. Ignoring the rotational level dependence of the quenching rate results in a lower local temperature of approximately 50 K. For this reason, the rotational level dependence of the quenching rate is always taken into account when determining the flame temperature for the low-pressure experiments described in this thesis.

As mentioned above, the results should also be corrected for the effects of fluorescence trapping and absorption. Desgroux et al. [22] give a computational method for correcting the OH-LIF temperature measurements for these effects. The corrections yield a typical adjustment of +30 K for the hot-gas temperatures reported in this thesis; this correction has been neglected in favor of using the overall estimated measurement uncertainty of ±50-75 K.

Following Berg et al [5], all measured temperature profiles are fit to an empirical equation:

$$T = A + B \cdot \left[1 - \exp\left(C \times h^{D}\right)\right] + E \times h^{2}, \qquad (3.19)$$

where A,B,C,D and E are fitting constants and h the height above the burner [mm]. The fitting procedure is performed using the subroutine LMDIF from the MINPACK library [25]. The results of the fit are used as input for the CHEMKIN calculations [28].

3.4.4 CH and OH concentration measurements using Rayleigh scattering

This paragraph discusses the determination of absolute CH and OH concentration. For converting relative LIF signals to absolute species concentrations, using equation (3.11) and the measured temperature and quenching rates, information on the geometrical factor $\left(l\frac{\Omega}{4\pi}\right)$ is needed. The geometrical factor depends on the experimental setup and can be determined most accurately using another spectroscopic technique. Here we use Rayleigh scattering for this purpose, following the procedure described by Luque et al. [15]. This procedure will be explained below using the determination of the absolute CH concentration as an example.

Rayleigh scattering is a process in which light is scattered elastically from molecules, i.e., with the same frequency as the incident light. The Rayleigh scattering signal, S_{RS} [photons], can be written as

$$S_{RS} = \frac{N\lambda_s}{hc} E_L \left(\frac{\delta\sigma}{\delta\Omega}\right)\Omega l, \tag{3.20}$$

where N is the number density of the scatterers, λ_s the wavelength of the scattered light, and $(\partial\sigma/\partial\Omega)$ the Rayleigh differential cross section. For a 90° scattering geometry, the Rayleigh differential cross section is expressed as [29]:

$$\left(\frac{\partial\sigma}{\partial\Omega}\right)_{90^\circ} = \frac{4\pi^2(n_i-1)^2}{\lambda_s^4 N_0^2}, \tag{3.21}$$

where n_i is the index of refraction of species i, at T=273 K and p = 1 atm, and N_o is the Loschmidt number.

The index of refraction (n_i) in equation (3.21) depends on the incident wavelength and can be calculated using Cauchy's equation [30]:

$$n_i = A_1\left(1+\frac{B_1}{\lambda_{scatt}^2}\right), \tag{3.22}$$

where A_1 and B_1 are constant specific for species i. The Rayleigh scattering is performed in N_2 where $A_1=2.92\times10^{-4}$ and $B_1=7.70\times10^{-5}$ [30]. Thus, once the wavelength of the scattered light is known, it is possible to calculate the differential cross section.

Equation (3.20) can be rewritten using the ideal gas law $(N = p/kT)$ to:

$$S_{RS} = D_{RS} P E_L, \tag{3.23}$$

where

$$D_{RS} = \frac{\lambda_s}{hc}\frac{1}{kT}\left(\frac{\partial\sigma}{\partial\Omega}\right)\Omega l. \tag{3.24}$$

The Rayleigh calibration is performed in N_2 at room temperature with excitation wavelength 435.4 nm, corresponding to the $P_{1e}(8.5)$ transition of the $A^2\Delta$-$X^2\Pi$ (0,0) band of CH (see Table 3.1). To determine the value of D_{RS}, the pressure of N_2 is varied between 200 and 5 Torr. The Rayleigh scattering signals are corrected for stray light and plotted against the product of laser energy and pressure, as shown in Figure 3.14.

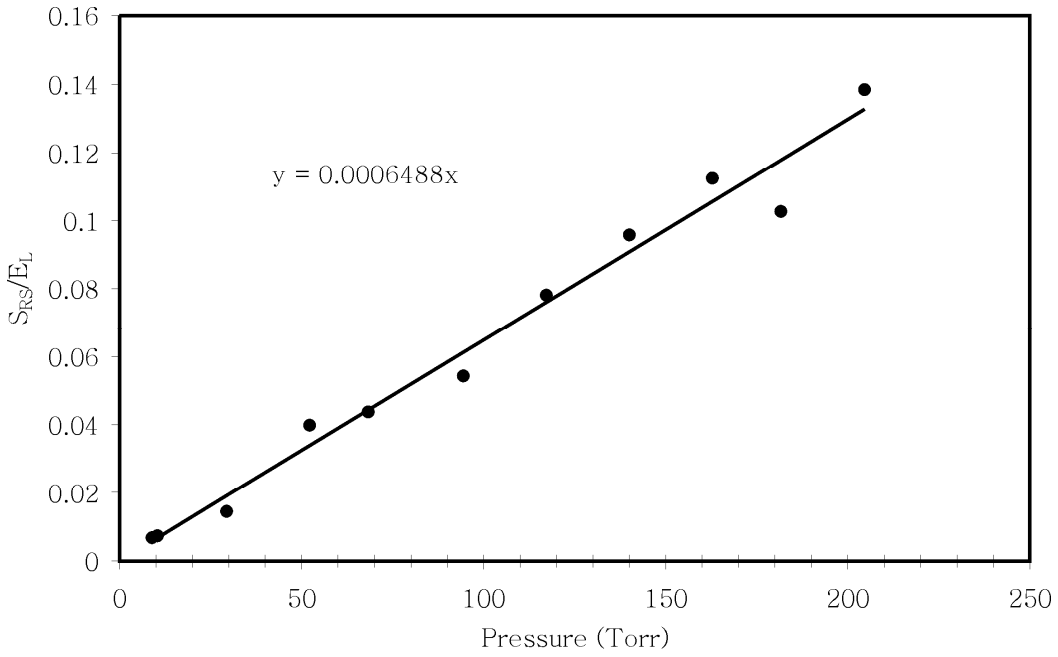

Figure 3. 14 The Rayleigh signal corrected for laser energy as function of the pressure. Also the result of fitting the data to a linear expression y=ax is plotted, where a = D_{RS} .

From equation (3.11), the following expression for the CH mole fraction can be derived:

$$X_{CH} = \frac{kT4\pi \cdot c^2 I_v}{P\Omega l \phi_u B_{du} f_d(T)\Gamma(v)E_L} \tag{3.25}$$

In order to save time, the integrated fluorescence signal F is measured at only one location in the flame (reference point) by scanning the laser line around the absorption transition. At this point, the convolution integral $\Gamma(v)$ at the frequency of the maximum of the absorption line, v_0, is determined by normalizing the fluorescence signal as:

$$\Gamma(v_0) = \frac{I(v_0)}{\int I(v)dv} = \frac{I(v_0)}{F}. \tag{3.26}$$

At other points, measurements of the fluorescence intensity are performed only at fixed laser frequency v_0, while the integrated fluorescence signal is calculated from expression (3.26) using the value $\Gamma(v_0)$ for the reference point.

Measurements and calculations show that under the experimental conditions in this study, the magnitude of $\Gamma(v_0)$ changes less than 5% from its average value of 3.42 cm^{-1}.

The measured CH signals show a substantial background (illustrated in Figure 3.15), originating from population in the upper electronic state $A^2\Delta$ created during chemical reaction (chemiluminescence).

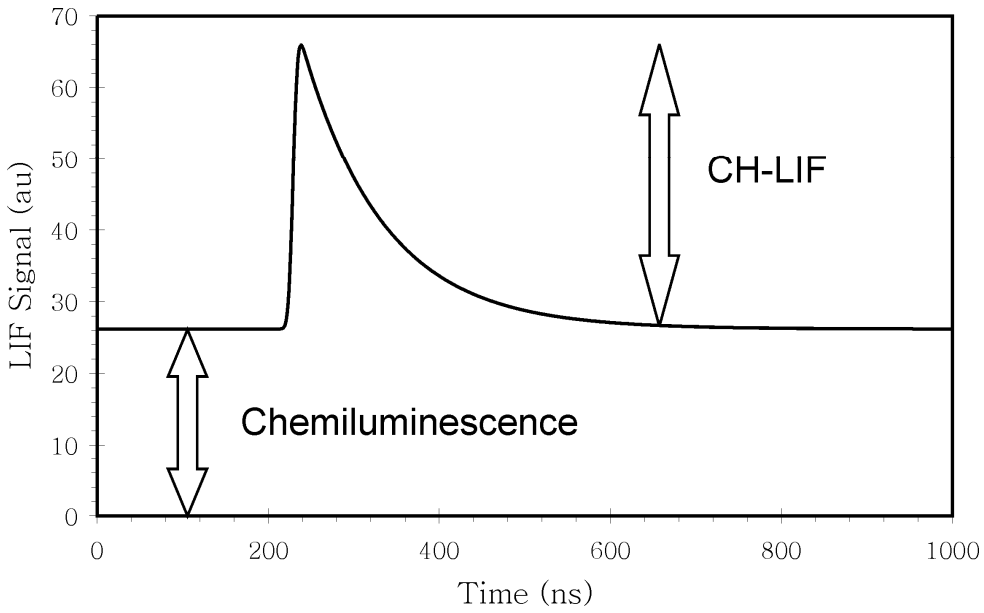

Figure 3. 15 Illustration of principle for determination CH-LIF signal

After subtracting the chemiluminescent background signal, the CH-LIF signal is integrated over time, as discussed above. The thus experimentally determined quenching rate of CH, temperature profile and geometrical parameter in equation (3.25) are used to determine the absolute CH concentrations at the maximum of the relative CH concentration profile. Table 3.4 summarizes the parameters used for the absolute determination.

Parameter	Value
T at CH maximum	1700 K
$F_d(T)$	0.020
A_u [31]	1.88×10^{6} s^{-1}
Q_u	1.19×10^{7} s^{-1}
ϕ_u	0.137
B_{du} [9]	1.34×10^{24} $cm^3J^{-1}s^{-1}$
p	25 Torr
$\Gamma(v)$	3.42 cm

Table 3. 4 Parameters used for calculation of the absolute peak CH concentration in the reference flame

The measurements are repeated several times, resulting in an average peak CH concentration in the reference flame of 10.6±1.8 ppm (95% confidence limit, 10 measurements). Subsequently, the vertical CH-LIF profile is calibrated to the CH peak concentration and corrected for temperature dependence. The result is shown in Figure 3.16, together with the measured temperatures, and are compared with the measurements in the same flame reported in the literature [5].

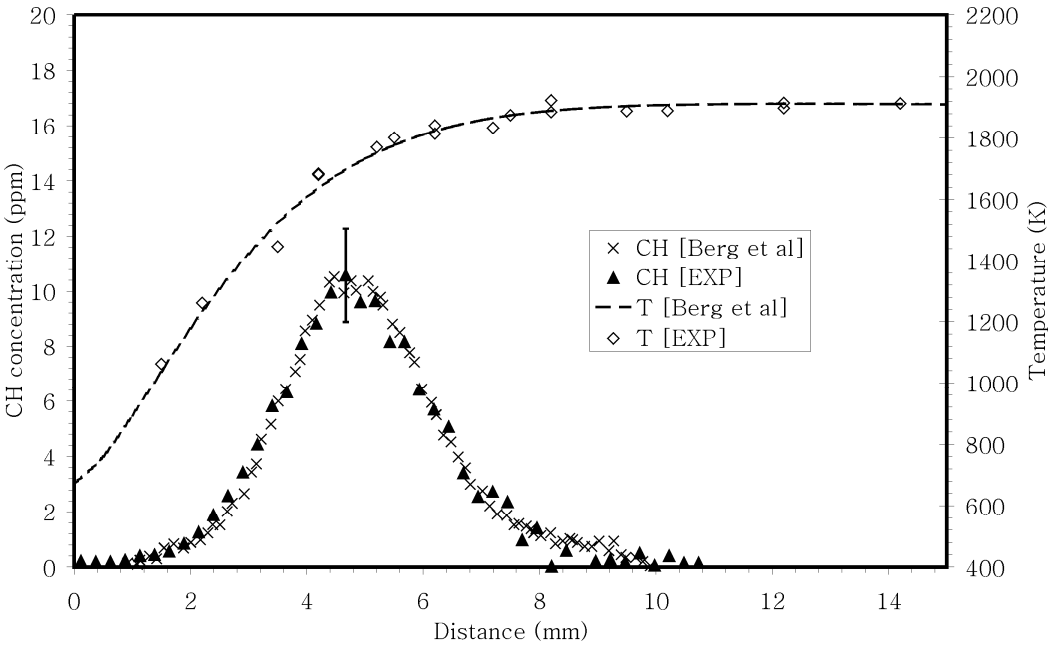

Figure 3. 16 Temperature and CH-concentration profile for the reference flame. The accuracy of the CH measurements (10.6 ± 1.8 ppm, 95% confidence limit) and temperature- and CH- profile measured by Berg et al [5] are also indicated in the Figure.

The measured CH profile is in excellent agreement with that determined by Berg et al [5], as is the mole fraction at the maximum of the profile (10.5 ± 1.7 ppm). Although this agreement is perhaps better than should be expected, given the cumulative uncertainties, it seems that following the methodology described in earlier work [15] does indeed lead to the reproduction of those results. Recent independent measurement [32] of the CH profile in the reference flame using another laser diagnostic technique, cavity-ringdown spectroscopy, suggests an accuracy of ~15%. Combined with the uncertainties in temperature, quenching and reproducibility of the measurements, we estimate the total uncertainty of the CH mole fractions to be better than 25%.

To avoid uncertainties in the effective path length caused by the boundary layer in low-pressure flames [32,33], the OH concentration in the reference flame is also determined using Rayleigh scattering, as described above. Measurements performed in the reference flame yield mole fractions within 10% of the value measured by Berg et al [5] of 12.000 ppm. The OH LIF intensity and mole fraction at 1.5 cm axial distance in the reference flame are

used as a calibration point for converting the relative OH profiles in the other flames to mole fractions, with an estimated accuracy of 20 %.

3.4.5 NO concentration in reference flame

The absolute NO concentration in the reference flame is determined following the procedure described by Berg et al [4], in which a small amount of NO is added to the cold gas mixture, and comparing LIF signals with and without seeding. As described in Chapter 2, a portion of the N_2 flow in the cold gas mixture is replaced by a gas mixture of 5021 ppm NO in N_2, resulting in 40-200 ppm in the cold gas mixture. In this way the flame temperature is unchanged compared to the non-seeded flame [4]. In addition, the quenching remains the same for seeded and non-seeded flame, since in these low concentrations the NO molecule has no significant influence on the NO quenching [10]. Consequently, the quenching and temperature terms in equation (3.12) can be treated as constants. With this in mind, the fluorescence signal can be rewritten as:

$$F = C \cdot [NO] \tag{3.27}$$

where $[NO]$ is NO concentration and C is proportionality coefficient. Assuming that the NO concentration in the seeded flame is the sum of NO concentrations in non-seeded flame and unburned mixture, the coefficient C can be found from the relation

$$C = \frac{F_{add} - F_{noadd}}{[NO]_{add}}, \tag{3.28}$$

where F_{add} and F_{noadd} are fluorescence signal in seeded and non-seeded flames, respectively. Model calculations using PREMIX code of CHEMKIN II package and GRI-Mech 3.0 indicate the NO added for calibration is reduced by 6% due to dilution and reburning [34], for which the data is corrected.

Using varying amounts of seed NO (40-200 ppm), the native NO mole fraction in the reference flame is determined to be 17.9±0.6 ppm (95 % confidence limit, 23 measurements) at 2 cm above the burner surface, which

corresponds remarkably well with the 17.5±0.5 ppm NO reported by Berg et al. [4] for the same conditions.

The NO concentration in flames other than the reference flame, are determined using the NO-LIF signal from the reference flame at 2 cm axial distance, where 40-50 ppm NO is added to enhance the signal. Based predominantly on the accuracy of the calibration gas, the estimated accuracy of the NO measurements is 15%.

Bibliography

1. Kohse-Hoinghaus, K., "Laser Techniques for the Quantitative Detection of Reactive Intermediates in Combustion Systems", *Prog.Energy Combust.Sci.* **20**, 203-279 (1994)

2. Eckbreth, A. C., *Laser diagnostics for combustion temperature and species*, (Taylor & Francis, New York, 1996)

3. Cheskis, S., "Quantitative Measurements of Absolute Concentrations of Intermediate Species in Flames", *Prog.Energy Combust.Sci.* **25**, 233-252 (1999)

4. Berg, P. A., Smith, G. P., Jeffries, J. B., and Crosley, D. R., "*Nitric Oxide Formation and Reburn in Low-Pressure Methane Flames*", 27th Symp. (Int.) Combust., 1377-1383 (1998)

5. Berg, P. A., Hill, D. A., Noble, A. R., Smith, G. P., Jeffries, J. B., and Crosley, D. R., "Absolute CH Concentration Measurements in Low-Pressure Methane Flames: Comparisons With Model Results", *Combust.Flame* **121**, 223-235 (2000)

6. Luque, J. and Crosley, D. R., "Radiative, Collisional, and Predissociative Effects in CH Laser-Induced-Fluorescence Flame Thermometry", *Appl.Opt.* **38**, 1423-1433 (1999)

7. Lee, M. P., Kienle, R., and Kohse-Hoinghaus, K., "Measurements of Rotational Energy Transfer and Quenching in OH A2S+, V'=0 at Elevated Temperature", *Appl.Phys.B* **58**, 447-457 (1994)

8. Daily, J. W., "Laser Induced Fluorescence Spectroscopy in Flames", *Prog.Energy Combust.Sci.* **23**, 133-199 (1997)

9. Luque, J. and Crosley, D. R., "LIFBASE: Database and spectral simulation (version 1.5)", SRI International Report MP 99-009, 1999

10. Tamura, M., Berg, P. A., Harrington, J. E., Luque, J., Jeffries, J. B., Smith, G. P., and Crosley, D. R., "Collisional Quenching of CH(A), OH(A), and NO(A) in Low Pressure Hydrocarbon Flames", *Combust.Flame* **114**, 502-514 (1998)

11. Sepman, A. V, Essen, V. M. van, Toro, V. V., Mokhov, A. V., and Levinsky, H. B.,"*Calibration of OH LIF Measurements by Direct Absorption in Laminar Premixed Lean CH4/Air flame*",in European Combustion Meeting 2005 Editors; J.Vandooren, Louvain-la-Neuve, Belgium, Paper 65, (2005)

12. Zabarnick, S and Alspach, D. A,"*Absolute concentration measurements of free radicals in flames by absorption spectroscopy"*,PL-TR-91-3012,(1979)

13. Pillier, L., Moreau, C., Mercier, X., Pauwels, J. F., and Desgroux, P., "Quantification of Stable Minor Species in Confined Flames by Cavity Ring-Down Spectroscopy:Application to NO", *Appl.Phys.B* **74**, 427-434-2002)

14. Sepman, A. V., Essen, V. M. van, Mokhov, A. V., and Levinsky, H. B., "Cavity Ring-Down Measurements of Seeded NO in Premixed Atmospheric-Pressure H-2/Air and CH4/Air Flames", *Appl.Phys.B* **77**, 109-117 (2003)

15. Luque, J. and Crosley, D. R., "Absolute CH Concentrations in Low-Pressure Flames Measured With Laser-Induced Fluorescence", *Appl.Phys.B* **63**, 91-98 (1996)

16. Rensberger, K. J., Jeffries, J. B., Copeland, R. A., Kohsehoinghaus, K., Wise, M. L., and Crosley, D. R., "Laser-Induced Fluorescence Determination of Temperatures in Low-Pressure Flames", *Appl.Opt.* **28**, 3556-3566 (1989)

17. Luque, J., Juchmann, W., and Jeffries, J. B., "Absolute Concentration Measurements of CH Radicals in a Diamond-Depositing Dc-Arcjet Reactor", *Appl.Opt.* **36**, 3261-3270 (1997)

18. Tamura, M., Luque, J., Harrington, J. E., Berg, P. A., Smith, G. P., Jeffries, J. B., and Crosley, D. R., "Laser-Induced Fluorescence of Seeded Nitric Oxide As a Flame Thermometer", *Appl.Phys.B* **66**, 503-510 (1998)

19. Battles, B. E. and Hanson, R. K., "Laser-Induced Fluorescence Measurements of No and Oh Mole Fraction in Fuel-Lean, High-Pressure (1-10Atm) Methane Flames - Fluorescence Modeling and Experimental Validation", *JQSRT* **54**, 521-537 (1995)

20. Wysong, I. J., Jeffries, J. B., and Crosley, D. R., "Laser-Induced Fluorescence of O(3P3P), O-2, and No Near 226 Nm - Photolytic Interferences and Simultaneous Excitation in Flames", *Opt.Lett.* **14**, 767-769 (1989)

21. Luque, J., Jeffries, J. B., Smith, G. P., and Crosley, D. R., "Combined Cavity Ringdown Absorption and Laser-Induced Fluorescence Imaging Measurements of CN(B-X) and CH(B-X) in Low-Pressure CH4-O-2-N-2 and CH4-NO-O-2-N-2 Flames", *Combust.Flame* **126**, 1725-1735 (2001)

22. Desgroux, P., Gasnot, L., Pauwels, J. F., and Sochet, L. R., "Correction of LIF Temperature Measurements for Laser Absorption and Fluorescence Trapping in a Flame", *Appl.Phys.B* **61**, 401-407 (1995)

23. Smith, G. P., Golden, D. M., Frenklach, M., Moriarty, N. W., Eiteneer, B., Goldenberg, W., Bowman, C. T., Hanson, R., Gardiner, W. C, Lissianski, V., and Qin, Z., http://www.me.berkeley.edu/gri_mech/.

24. Kreyszig, E., *Advanced Engineering Mathematics*, (John Wiley & Sons, New York, 1993)

25. More, J. J., Garbow, B. S., and Hillstrom, K. E., "User Guide for MINPACK-1", Argonne National Laboratory Report ANL-80-74, Argonne, Ill., 1980

26. Jeffries, J. B., Kohse-Hoinghaus, K., Smith, G. P., Copeland, R. A., and Crosley, D. R., "Rotational-Level-Dependent Quenching of OH(A2S+) at Flame Temperatures", *Chem.Phys.Lett.* **152**, 160-166 (1988)

27. Cattolica, R. J. and Mataga, T. G, "Rotational-Level-Dependent Quenching of OH A2S+(v'=1) by Collisions With H2O in a Low-Pressure Flame", *Chem.Phys.Lett.* **182**, 623-631 (1991)

28. Kee, R. J., Rupley, F. M., and Miller, J. A., "CHEMKIN II: A Fortran Chemical Kinetics Package for the Analysis of Gas-Phase Chemical Kinetics", Report No.SAND89-8009, Sandia National Laboratories ,1989

29. Zhao, F. Q. and Hiroyasu, H., "The Applications of Laser Rayleigh-Scattering to Combustion Diagnostics", *Progress in Energy and Combustion Science* **19**, 447-485 (1993)

30. Born, Max, Wolf, Emil, and Bhatia, A. B., *Principles of optics : electromagnetic theory of propagation, interference, and diffraction of light*, (Pergamon Press, Oxford ; New York, 1975)

31. Luque, J. and Crosley, D. R., "Electronic Transition Moment and Rotational Transition Probabilities in CH.I A2D-X2P System", *J.Chem.Phys* **104**, 2146-2155 (1995)

32. Luque, J., Berg, P. A., Jeffries, J. B., Smith, G. P., Crosley, D. R., and Scherer, J. J., "Cavity Ring-Down Absorption and Laser-Induced Fluorescence for Quantitative Measurements of CH Radicals in Low-Pressure Flames", *Appl.Phys.B* **78**, 93-102 (2004)

33. Pillier, L., El Bakali, A., Mercier, X., Rida, A., Pauwels, J. F., and Desgroux, P., "*Influence of C-2 and C-3 Compounds of Natural Gas on NO Formation: an Experimental Study Based on LIF/CRDS Coupling*", 30th Symp. (Int.) Combust., 1183-1191 (2005)

34. Sepman, A. V., *Effects of the burner stabilization on nitric oxide formation and destruction in atmospheric-pressure flames*, Rijksuniversiteit Groningen, 2006